Application of a valveless impedance pump in a liquid cooling system

Chih-Yung Wen[a,*], Shi-Jung Yeh[b], Kuok-Pong Leong[b], Wei-Shen Kuo[b], Howard Lin[c]

[a]Department of Mechanical Engineering, The Hong Kong Polytechnic University, Kowloon, Hong Kong
[b]Department of Aeronautics and Astronautics, National Cheng-Kung University, Tainan, Taiwan 701
[c]Innovative Technical Center, Cooler Master Co., Ltd., Taipei, Taiwan 235

Abstract

In this study, a novel valveless impedance pump is applied, for the first time, in the thermal management of high performance electronic systems. This small pump comprises an amber latex rubber tube, connected at both ends to rigid copper tubes of different acoustic impedance, and a simple, economic, quiet and energy–efficient actuation mechanism, which combines a small DC motor and a cam. The motor activated cam periodically compresses the elastic tube at a position asymmetric from the tube ends. Traveling waves, emitted from the compression, combine with reflected waves, at the impedance-mismatched positions (rubber tube/copper tube interfaces). The resulting wave interference creates a pressure gradient, with the potential to generate a net flow. Several experimental set–ups for performance tests, using a single impedance pump, open system, with isothermal flow, and a closed liquid cooling system were designed and implemented. The performance of the impedance pump was affected significantly by the actuation

frequency (input voltage) and position. The pump flow rate varied nonlinearly with the actuation frequency. The measured maximum flow rate of the current design is 480 ml/min at zero total pump head, for operating frequencies in the range 48–63 Hz. The water–cooling system in a closed loop maintains the core temperature of the 60 W dummy heater at 57.8 °C. Experimental results demonstrate the feasibility of the commercial application of valveless impedance pumps for thermal management in high performance electronic systems.

Keywords: Thermal management; valveless impedance pump; liquid cooling

*Corresponding author, Tel: (852) 27666644   Fax: (852) 23654703

E-mail address: chihyung.wen@polyu.edu.hk (C.Y. Wen)

Nomenclature

A	Cross-section area
D	Average diameter of the elastic tube
f	Actuation frequency in Hz
H	Water head in Pa
h	Water head in cm
L	Length of the elastic tube
Q	Flow rate
Q_{cpu}	Dummy heater power
R	Flow resistance
T	Temperature
T_h	Temperature of the heater
$T_{h,in}$	Temperature of the inlet in the cold plate
$T_{h,out}$	Temperature of the outlet in the cold plate
T_R	Temperature of the radiator
$T_{R,in}$	Temperature of the radiator inlet
$T_{R, out}$	Temperature of the radiator outlet
$T_{p,in}$	Temperature of the pump inlet
V	Voltage applied to the motor in Volt
v	Flow velocity
x, y	Coordinates

Z   Acoustic impedance

1. Introduction

In recent years, thermal management in high performance electronic systems, such as Central Processing Units (CPU) and Graphics Processing Units (GPU) in desktops, cloud computing servers and laptops, has become more important, due to the increase in heat generated within such systems. A system's performance and reliability is strongly dependent on its temperature control. Among many passive and active cooling solutions, liquid cooling, which can remove a large amount of heat, has attracted considerable attention among industry engineers studying next–generation thermal management solutions. Micro–pumps, with their advantages of small size, configurable dimensions and low power consumption and noise, have emerged as the driving device of choice, for liquid cooling.

In general, micro–pumps can be classified as either mechanical or non–mechanical, depending on their mode of operation. Mechanical micro-pumps can be further classified as either displacement or dynamic types. Displacement micro–pumps are either reciprocating (diaphragm), or peristaltic pumps. The former type incorporates an actuator-driven pressure chamber and mechanically operated inlet and outlet passive check valves [1–4]. However, the movable valves render the micro-fluidic system prone to mechanical failure, which can result in fluid leakage at high operating pressures.

In an attempt to resolve these problems, researchers have proposed a variety of valveless peristaltic micro pump schemes [5, 6], or reciprocating diaphragm pumps, integrated with nozzles/diffusers [7–11]. Such systems are generally fabricated on a substrate, using MEMS techniques, and are not intended to provide a high flow rate in a closed system with flow resistance. More recently, a novel valveless scheme, based on impedance mismatch effect, has also been presented, which allows a relatively high pumping rate and simpler structure, compared with the two valveless schemes already mentioned [12–14]. Rinderknecht *et al* [12] proposed a novel valveless, substrate-free impedance-based micro pump driven by an electromagnetic actuating force. In their closed circuit flow configuration, the pump was constructed of an elastic silicone tube of inner diameter 2 mm and wall thickness 50 μm, coupled at both ends to rigid glass capillary tubes. The important features of the substrate-free construction and the absence of complex parts and inner geometries make the impedance pump well suited for integration into cost-focused, space limited applications including drug delivery, cell sorting, chemical analysis as well as act to complement current stenting and shunting techniques. The performance of the pump was found to be highly sensitive to the waveform, offset, amplitude and duty cycle of the excitation force. Upon the promising demands for biomedical devices on the microscale as well as applications involving

chemical control, mixing and analysis, Wen et al. [13] presented a planar valveless micro impedance pump in which a PZT actuator was used to drive a thin Ni diaphragm at its resonance frequency of 34.7 kHz for lab-on-chip (LOC) integrated systems. The resulting large-scale displacements of the diaphragm created a significant driving pressure and yielded a substantial net flow. Lee et al. [14] designed and fabricated another planar micro impedance pump in an open configuration, driven by the electromagnetic actuator. The micro pump comprised four major components, namely a lower glass substrate containing a copper micro coil, a microchannel, an upper glass cover plate and a PDMS diaphragm with a magnet mounted on its upper surface.

The impedance pumping phenomenon was first observed by Liebau [15] in 1954 when he tried to explain why, during early embryonic life, blood circulates in one direction, in spite of the complete lack of valves, and how the valveless hearts of some adult invertebrates function. In his series of experiments [15–18], he used elastic tubes with different diameters and different elastic properties and demonstrated the occurrence of a valveless pumping effect. Therefore, the impedance–pumping phenomenon is sometimes referred to as Liebau phenomenon. His discoveries stimulated several analytical, computational and more comprehensive experimental investigations of this pumping mechanism [19–30] in cardiovascular dynamics. These works have been excellently reviewed by Manopoulos et al. [19]. For example, in 1978, Thomann [20] used the method of characteristics in conjunction with numerical computations to study a

simple torus model consisting of an elastic tube and a rigid tube joined together (such a model was physically reconstructed in a more recent work by Moser et al. [21]). In 2003, Ottesen [24] derived a one-dimensional (1-D) nonlinear mathematical model for a fluid-filled torus by averaging the Navier–Stokes equations. The mathematical model was then analyzed partly analytically and partly numerically. His theoretical findings were validated by a series of experiments carried out on a physical realization of the torus system. It was observed that (1) a remarkable unidirectional mean flow in the torus was produced by compressing the soft tube at an asymmetric site with respect to the system's configuration and (2) the size and direction of the mean flow depend on many factors in a complicated manner, such as the frequency and specific temporal form of the compression, the elasticity of the tubes, the compression ratio...etc. Hickerson et al. [26] constructed an impedance pump by connecting an elastic tube to two water reservoirs and carried out a comprehensive experimental study to answer a number of important questions regarding the fundamental mechanisms of valveless pumping; in some experiments, the two reservoirs were also connected by an additional rigid tube to form a closed-loop system. The elastic tube was compressed by a set of pinchers moving sinusoidally at a controllable frequency and fixed duty cycle. Several distinctive features of the impedance-driven flows were demonstrated. In particular, it was observed that the net flow is highly sensitive to the pinching frequency and a pressure head can be created in an open-loop system. Hickerson and Gharib [27] continued to propose a simple 1-D "wave-pulse model" accounting for wave amplitude attenuation and reflection at impedance mismatched

interfaces in an impedance pump; the model predicted many of the characteristics exhibited by the experiments of Hickerson et al. [26]. A more sophisticated numerical FSI (Fluid and Solid Interaction) study was further conducted by Avrahami and Gharib [28], to investigate further the wave dynamics in impedance pumps. More recently, Huang et al. [30] presented an analytical model for a valveless micro impedance pump driven by PZT actuation. A one-dimensional wave equation was developed for acoustic pressures in the compressible section, taking into account the actuations as acoustic source terms. The solution for the acoustic pressure was a set of standing waves established inside the compressible section, corresponding to the actuations. The pumping effect was attributed to the second-order terms of the acoustic pressures. Two control parameters were identified: (1) the resonance frequency associated with the sound wave speed and length of the compressible section, and (2) the damping factor. The analytical results were compared with the experimental data of Wen et al. [13], and a qualitative agreement was observed in terms of frequency characteristics of the pumping pressure.

To Summarize, the valveless impedance pump normally takes the form of a flexible section, connected at either end to two rigid sections of different acoustic impedance, as depicted in Fig. 1. The impedances of the flexible and two rigid sections are represented by Z_0, Z_1 and Z_2, respectively. In this pump, the elastic section is periodically compressed, at a position, asymmetric from the ends, with a motor-actuated cam. Traveling waves, emitted from the compression, combine with reflected waves at the

impedance-mismatched positions. The resulting wave interference generates a pressure gradient, with the potential to generate a net flow – typically pulsing – within the fluid system. The performance of the pump is found to be highly sensitive to the impedance mismatch (materials) and waveform, offset, amplitude and duty cycle of the excitation force, and generally exhibits two distinguishing features: (1) a nonlinear response to the actuating compression frequency and (2) reversal of flow direction at certain frequencies. Contrarily, the flow in a peristaltic system increases linearly with the actuation frequency and runs only in the direction of compression. Therefore, it is important to calibrate the impedance pump and find the optimal operational parameters (compression position, amplitude and frequency) that can generate the maximum flowrate for cooling.

In literature, various actuation mechanisms have been proposed for micro–pumps, including piezoelectric [3, 8, 13, 31], electromagnetic [2, 12, 14, 32–36], thermo-pneumatic [37, 38], electrostatic [39, 40], and the use of shape–memory alloys [41, 42]. However, piezoelectric and electrostatic membrane actuators require a high voltage to achieve a sufficient membrane displacement. An extra high–voltage electronic power system is needed. Furthermore, electrostatic forces are only effective over a range of several micrometers. Unfortunately, thermo–penetration and shape memory alloy actuators provide only a limited actuation frequency, so the attainable output from the

micro-pump is low. Therefore, the practicability of these actuation mechanisms is limited in liquid cooling systems.

Accordingly, this study presents and analyzes a valveless impedance pump, and focuses specifically on demonstrating its commercial feasibility for thermal management in high performance electronic systems. A simple, economic, quiet and energy–efficient actuation mechanism, combining a small DC motor and a cam, is presented.

2. Development of the valveless impedance micro–pump and experimental set up

2.1 Valveless impedance micro–pump

Figure 1 shows a schematic illustration of the impedance pump developed in this study. As shown, the pump comprises an elastic amber latex rubber tube, of circular cross–section, connected at either end to two rigid copper tubes. The amber latex rubber tube was chosen because of its good wear–resistance and thermal aging characteristics. The elastic tube has a length of 80 mm, an outer diameter of 6 mm, an inner diameter of 4 mm, and wall thickness of 1.0 mm. The copper tubes have an outer diameter of 4.8 mm, an inner diameter of 4.2 mm, and a wall thickness of 0.3 mm. An electro-mechanical actuating mechanism, with a small motor–driven cam, was used to compress the elastic tube at various locations along its length ($x/L=1/8$, 2/8 and 3/8, see Fig. 1), at various

compression frequencies (f), with fixed amplitudes $\Delta y/D = 1$ (*i.e.* complete closure of the elastic tube). According to earlier experimental studies [26, 29], $\Delta y/D = 1$ yields the maximum flow rate at any f, with various compression amplitudes $\Delta y/D$.

The detailed dimensions of the cam are shown in the upper–right inset of Fig. 1. The corresponding duty cycle (*i.e.* the fraction of the time the cam is in contact with the elastic tube wall in an actuating period) is 36%. The cam is made of PTFE, because of its good lubrication characteristics under dry contact. A small DC motor (FM-2088, Tricore Corp., Taiwan), with dimensions of 16 mm × 8 mm × 6 mm (length × width × height), was used to drive the cam and compress the elastic tube. The power needed by this motor is about 1.5 W. Note that an electro–mechanical compression mechanism was chosen in the current study, because it offers the possibility of large displacements (ranging from a few millimeters to a few centimeters), with low power consumption, in a quiet, simple, economical way.

2.2 Experimental set–up for pump performance

Figure 2 is a schematic illustration of the experimental setup used to characterize the pump. To measure mass flow rate profiles for the pump, obtained at different actuation

frequencies, the pump was connected to a water reservoir at one end, while the other end was left open, to drain the water (Fig. 2(a)). To measure the pumping pressures (water heads), the two copper tubes at both ends of the pump were connected to two acrylic reservoirs, using CCP-CA-260 adhesive (Fig. 2(b)). The reservoirs had a length of 400 mm, an outer diameter of 14 mm, an inner diameter of 12 mm, and a wall thickness of 1 mm.

As shown in Fig. 2(b), the major items of experimental hardware comprise a programmable DC power supply (MOTEH Co., Taiwan, LPS-305), a digital oscilloscope (Tektronix, TDS 2014), a stroboscope (Strobotac 1546), and a CCD camera interfaced to a PC. The application of a power supply to the electric motor causes the cam to compress the elastic tube. The digital oscilloscope was used to monitor the actuation voltage. At the beginning of each experiment, the pump was filled with water and the relationship between the actuation frequency, f, under load and the voltage applied to the motor, V, were first calibrated with the stroboscope. The pulse length of the flash is approximately 1.2 μs, which is sufficiently short to freeze the motion of the cam when the correct flashing frequency is set. When performing a linear regression analysis, a relationship was found between f and V:

$$f = 5\,V - 2$$

for 10 Volts $\leq V \leq$ 13 Volts, with a high correlation coefficient (R^2 value of the fit) of 0.998. Because the programmable power supply (PROVA-8000, TES Electrical Electronic

Corp., Taiwan) was used to apply voltage to the motor, with the voltage accuracy of 0.1 %, the uncertainty of frequency was estimated to be 0.1 %, accordingly. The DC voltage range between 10 and 13 Volts was chosen, because the voltages of the DC power supplies for fan cooling in most desktops, cloud computing servers and laptops are around 12 Volts. The pump was designed to be powered by the same DC power supply as that used for water–cooling in high performance electronic systems, so that no extra power/control electronics are needed.

The response of the pump flow rate to the actuation frequency was measured afterward (Fig. 2(a)). The water reservoir and the pump tubing were filled with water initially, with the ball valve closed. The water level in the reservoir was 1.0 cm above the pump, to minimize the initial pressure head. When the pump was activated, the valve was opened and the water flow rate was calculated by measuring the volume of water collected in the sink, after 10 seconds. The water flow rate was measured for every 1 Hz of frequency change.

Once the maximum water flow rate was found for a specific compression frequency, the pump head was measured at this optimal flow rate condition (Fig. 2(b)). The pump was filled with a mixture of water and methylene blue dye, until both reservoirs were filled to a half-height (equilibrium) position. After the pump was turned on, the pressure

head was measured, using a CCD camera to record the height difference between fluid columns in the two reservoirs, when the fluid levels in the reservoirs stabilized.

2.3 Set–up for thermal performance of the water-cooling system

Figure 3 shows the schematic and the picture of a water–cooling system in a closed loop, analogous to that used in a desktop, or notebook computer, for the thermal performance measurements. In this closed circulation system, air is carefully excluded from the pipe or the components. The copper chamber of the cold plate with six parallel fins is installed over the dummy heater. The dimensions of the fins and cold plate chamber are 30 mm (length) × 1 mm (width) ×2.5 mm (height) and 45 mm (length) × 28 mm (width) × 4 mm (height), respectively.

The working fluid is pumped through a copper cold plate chamber, in which the heat exchange takes place, carrying away heat from the dummy heater. An aluminum radiator then dissipates the heat. The interface of the cold plate and the dummy heater is smeared with thermal grease. The cold plate and the dummy heater are then fixed together with screws, using a torque wrench. The heat inputs to the dummy heater were provided by the programmable power supply (PROVA-8000, TES Electrical Electronic Corp., Taiwan). In the experiments, the constant current mode was adopted and the current was set at 2 A.

The wattage was determined by multiplying electric current by voltage applied to the dummy heater. Different wattage was obtained by adjusting the voltage applied. The accuracy of current and voltage are 0.2 % and 0.1 %, respectively, which yields a 0.3 % uncertainty of wattage. The top of the dummy heater was exposed to air to simulate the actual operation condition of a CPU or a GPU; hence the electrical heating was also carried away by the naturally convective air. Therefore, the wattages quoted are greater than the actual energy dissipated by liquid cooling due to these minor losses. In order to improve the dissipation efficiency of the radiator, a fan with a power supply of 12 V × 0.3 A is applied to the radiator.

Seven K-type thermocouples (with the accuracy of $0.15°C$) are used to record the temperature variations at different points in the circulation cooling system, with the heat inputs to the dummy heater from 5 W to 60 W, at 5 W intervals. As shown in Fig. 3, T_h, $T_{h,in}$, $T_{h,out}$, T_R, $T_{R,in}$, $T_{R,out}$, and $T_{p,in}$ represent the temperature of the heater, of the inlet and outlet in the cold plate, of radiator, of the inlet and outlet in the radiator and of inlet in the pump, respectively.

2.4 Set–up for flow rate performance of the water–cooling system

To measure the total head loss and flow rate performance in the simulated water–cooling system, the closed circulation loop in Fig. 3 (a) was opened at the pump inlet. Figure 4 presents this open system, in which water is pumped from the reservoir and then flows through the cold plate and radiator, before being drained into the sink (see also Electronic Annex 1, in the online version of this document.). Similarly to Fig. 2(a), the water level in the reservoir was slightly above the pump, to minimize the initial pressure head. When the pump was activated, the valve was opened and the water flow rate was calculated by measuring the volume of water collected in the sink after 10 seconds. Water flow rates were recorded at frequency intervals of 1 Hz.

3. Results and Discussion

3.1 Effects of actuation frequency and position on pump flow rates

Using the experimental set up, shown in Fig. 2(a), Fig. 5 illustrates the variation in the pump flow rate with the actuation frequency, as a function of the compression position at a constant compression amplitude of $\Delta y/D = 1.0$ (complete closure of the elastic tube). The pump flow rate was found to vary nonlinearly with the actuation frequency, for a constant compression position. Positive flow rate indicates that the fluid is driven from the

reservoir on the right–hand side of the pump to the left–hand side. Over the applied frequency range, no flow reversal effect was induced. The unique frequency dependence of the net flow rate, at different compression positions, implies an impedance-driven flow. It was also evident that the impedance pumping effect (*i.e.* the pump flow rate) was most significant as the compression location approached the elastic tube / copper tube interface. Note that the repeatability of the flow rate measurements is very high. For each experimental condition, the flow rate measurements were repeated for 5 times and 0.5% uncertainty was obtained.

A maximum pump flow rate of $Q = +480$ ml/min (at zero total pump head) was obtained, when the actuation force was applied at location $x/L = 1/8$, with a frequency of 51Hz (corresponding to an applied voltage, at the motor, of 10.6 volts). As the position of the pincher location moved toward the center of the elastic section, the pump flow rate decreased at $x/L = 2/8$ and then increased at $x/L = 3/8$. These observations indicate different interfering waveforms at different compression positions. Note that a flow was not produced when the elastic tube was compressed at its center since the transmitted waves caused by the compression effect were cancelled out by the waves reflected from the two elastic tube / copper tube interfaces. For an illustration of pressure waveform patterns along the length of the pump for varying time, please refer to Fig. 3 in reference [27].

3.2 Pump heads at optimal flow rate performance

Figure 6 shows the corresponding variation of pressure head with elapsed time, at the optimal flow rate performance, with an actuation frequency of 51 Hz and actuation position x/L = 1/8. It can be seen that the pressure increases rapidly, when the pump is turned on, and reaches a steady maximum pressure head of 0.62 m (6100 Pa), after an elapsed time of 60 seconds.

Böhm et al. [32] developed a plastic micro-pump with a valve (12 mm×12 mm×2 mm). A pumping rate of 2 ml/min and a pressure head of $1.25×10^4$ Pa were reached. Ma et al. [4] designed a one-side actuating piezoelectric micro-pump (45 mm×28mm×4mm), which is combined with a cold plate chamber, to drive water in a cooling system for a laptop. The measured maximum flow rate of this micro-pump was 246 ml/min, and its maximum pressure head reached 9807 Pa. A commercial product of SDMP305D（25 mm×25 mm×4.8mm）with central-actuating (Star Micronics Co. [43]), is a thin, compact, and lightweight piezoelectric micro-pump. Its maximum flow rate and maximum pressure head are 5 ml/min and $1.0×10^4$ Pa, respectively. The current valveless impedance pump provides a higher maximum flow rate than those of the three existing micro-pump technologies, with a comparable maximum pressure head. Further optimization on the pressure head will be pursued.

The H–Q (pressure head–flow rate) characteristic of the pump design, at an actuation frequency of 51 Hz and actuation position $x/L = 1/8$, is presented in Fig. 7. The flow velocities, v, at different pressure heads, were estimated first, by taking the time derivatives of the pressure head (Δh) – elapsed time curve, in Fig. 6. The corresponding flow rates were then determined by $Q = |v| \times A$, where A is the cross-sectional area of the observational acrylic reservoirs (see Fig. 2(b)). As shown, the pump flow rate decreases linearly, to a good degree, while pressure head increases. Note that the calculated flow rate, at zero total pump head, is 483 ml/min, which is consistent with the maximum flow rate (480 ml/min) measured in Fig. 5.

3.3 Flow rate performance and head loss in a water–cooling system

Figure 8 compares the measured flow rates of the water–cooling system in an open loop (Fig. 4) with that of the pump alone (Fig. 2(a)), at different actuation frequencies and optimal actuation position $x/L = 1/8$. It is evident that the variation of the flow rate with the actuation frequency, for the open loop, exhibits a broadly similar trend to that of the pump alone, although the magnitude is smaller (~ 100 ml/min, on average).

As mentioned in the introduction, a pair of waves is emitted in opposite directions each time the tube is compressed. In general, these waves are allowed to travel along the

tube and are then partially reflected in accordance with the relative impedances of the two materials when they propagate through the intersection between two media with different impedances. In the current experiments, the wave speed is around 50–60 m/s, or less, in a pliable latex rubber tube [27], which is much less than the normal speed of sound (1500 m/s) through water inside copper tubes. Therefore, the pressure waves inside the pumping section, propagating to both ends, will be almost totally reflected, as if they were propagating from a soft medium to a very hard one. Each wave pulse shape is then reflected in the same manner as the wave position if it crosses a reflection site. For each wave pair emitted, its start time, travel time, total distance traveled, directions, amplitudes, and positions are dependent on the compression period and which cycle it belongs to. All of the waves are finally summed along the length of the compression tube. Once equilibrium is reached, the mean value of the difference in the summed pressure wave amplitude at the ends of the line represents a value proportional to the pressure head of a similar pump and generates a net flow within the flow channel. Therefore, the pump curve is mainly dependent on the specific piping configuration and actuation parameters. Different materials, length of the pliable tube, actuating wave pulse shapes, actuating positions and actuating frequencies will all affect the pump performance. The constant decrease of the flow rate in Figure 8 is, hence, caused by the head losses in the copper

tube, bends, and cold plate of the water–cooling system, in an open loop.

At an actuation frequency of 51 Hz and actuation position x/L = 1/8 (see Figs. 7 and 8), the total pump head H_{pump} = 6100 Pa = $Q_{pump} \times R_{pump}$ = $Q_{open\,loop} \times (R_{pump} + R_{open\,loop})$, where Q_{pump} is the flow rate of pump alone, R_{pump} is the internal pump flow resistance, $Q_{open\,loop}$ is the flow rate of the open loop case, and $R_{open\,loop}$ is the total flow resistance of the copper tube, bends, and cold plate of the water–cooling system, in an open loop. Consequently, the pressure head loss in the open system, $Q_{open\,loop} \times R_{open\,loop}$ = $H_{pump} \times (1 - Q_{open\,loop} / Q_{pump}) \sim$ 6100 Pa $\times$ (1 $-$ 375 (ml/min) / 480 (ml/min)) = 1330 Pa. Optimal water–cooling systems will be necessary, in order to reduce pressure head loss in future practical applications.

3.4 Thermal performance of the water–cooling system in a closed loop

The study focuses on the thermal performance of a water–cooling system in a closed loop, at an actuation frequency of 51 Hz and actuation position x/L = 1/8. The relation between the heat generated in a dummy heater and its core temperature is shown in Fig. 9. The result shows that every measured temperature rises as its operating power increases, including the temperature of the heater (T_h), of the inlet and outlet in the cold plate ($T_{h,in}$ and $T_{h,out}$), of radiator (T_R), of the inlet and outlet in the radiator ($T_{R,in}$ and $T_{R,out}$) and of

inlet in the pump ($T_{p,in}$). These temperatures were recorded when they showed no variation over a period of 10 minutes and it was assumed that steady-state operating conditions had been reached.

The proposed cooling system maintains the core temperature in the dummy heater at 43.0 °C at 30 W operating power. When the power reaches 60 W, the core temperature rises to 57.8 °C.

4. Conclusions

A new valveless pump, based on impedance pumping, has been successfully developed and applied to the thermal management of high performance electronic systems. The pump composed an amber latex rubber tube, connected at both ends to rigid copper tubes of different acoustic impedance and a simple and economic actuation mechanism, combining a small DC motor and a cam. By periodically compressing the pliable rubber tube, at location asymmetric from the rigid ends, a net flow was generated to dissipate system heat successfully. The pump's performance was observed to be highly dependent on actuation frequency and position, for a fixed waveform, duty cycle and input excitation amplitude. It shows the following conclusions:

1. The measured maximum flow rate of the impedance pump is 480 ml/min at zero pump

head in the range of motor actuation voltage 10–13 Volts (corresponding operation frequency 48–63 Hz), which can be provided directly by the DC power supplies in most desktops and laptops. This optimal flow rate performance occurs at an actuation frequency of 51 Hz and actuation position $x/L = 1/8$.

2. The head of the small valveless impedance pump can reach 0.62 m.

3. The variation of the flow rate with the actuation frequency, for the open loop scenario (Fig. 4), exhibits a broadly similar trend to that of the pump alone (Fig. 2(a)). The head losses in the copper tube, bends, and cold plate of the water–cooling system in an open loop result in a constant decrease in the flow rate (~ 100 ml/min). Optimal water–cooling systems will be necessary, in order to reduce the pressure head loss in future practical applications.

4. The water–cooling system in a closed loop maintains the core temperature of the 60 W dummy heater at 57.8 °C. It is sufficient to the heat dissipation needs of current laptops, at full speed operation.

Impedance–based pumping presents an exciting new opportunity in active thermal management systems. Experimental results demonstrate the feasibility of its commercial applications in the thermal management of high performance electronic systems. Although

it is conceptually simple, significant future work is necessary to optimize its performance, including the proper choice of the flexible tube material to extend the pump life, and to maximize the impedance mismatch and flow rate accordingly. The optimal length of the flexible tube, actuation frequency and position need also to be found for the new combination of the impedance pump to expand the heat removal range. Notably, the amber latex rubber tube used in this study has problems of aging and hardening after hours of cooling and low resistance to friction rubbing by the compressing cam.

Acknowledgement

Reference

[1] R. Zengerle, J. Ulrich, S. Kluge, M. Richter, "A. Richter, A bidirectional silicon micropump," Sens. Actuat. A, vol.50, pp. 81–86, 1995.

[2] Q.L. Gong, Z.Y. Zhou, Y.H. Yang, X.H. Wang, "Design, optimization and simulation on microelectromagnetic pump," Sens. Actuat. A, vol.83, pp. 200–207, 2000.

[3] H.K. Ma, B.R. Hou, C.Y. Lin, J.J. Gao, "The improved performance of one-side actuating diaphragm micropump for a liquid cooling system," International Communications in Heat and Mass Transfer, vol.35, 957–966, 2008.

[4] H.K. Ma, B.R. Chen, J.J. Gao, C.Y. Lin "Development of an OAPCP-micropump liquid cooling system in a laptop," International Communications in Heat and Mass Transfer, vol.36, 225–232, 2009.

[5] J.M. Berg, R. Anderson, M. Anaya, B. Lahlouh, M. Holtz, T. Dallas, "A two-stage discrete peristaltic micropump," Sens. Actuat. A, vol.104, pp. 6–10, 2003.

[6] B. Husband, M. Bu, A.G.R. Evans, T. Melvin, "Investigation for the operation of an integrated peristaltic micropump," J. Micromech. Microeng., vol.14, pp. S64–S69, 2004.

[7] A. Olsson, P. Enoksson, G. Stemme, E. Stemme E, "A valveless planar pump isotropically etched in silicon," J. Micromech. Microeng. vol.6, pp. 87–91, 1996.

[8] A. Olsson, P. Enoksson, G. Stemme, E. Stemme E, "Micromachined flat-walled valveless nozzle pumps," J. Microelectromech. Syst., vol. 6, pp 161–166, 1997.

[9] X.N. Jiang, Z.Y. Zhou, X.Y. Huang, Y. Li, Y. Yang, C.Y. Liu, "Micronozzle/diffuser flow and its application in micro valveless pumps," Sens. Actuat. A, vol.70, pp. 81–87, 1998.

[10] H. Anderssona, W. van der Wijngaart , P. Nilsson, P. Enoksson, G. Stemme, "A valve-less diffuser micropump for microfuidic analytical systems," Sens. Actuat. B, vol. 72, pp 259–265. 2001.

[11] C.G.J. Schabmueller, M. KochM, M. E. Mokhtari, A.G.R. Evans, A. Brunnschweiler, H. Sehr, "Self-aligning gas/liquid micropump," J. Micromech. Microeng., vol 12, pp. 420–424, 2002.

[12] D. Rinderknecht, A.I. Hickerson, M. Gharib, "A valveless micro impedance pump driven by electromagnetic actuation," J. Micromech. Microeng., vol. 15 pp. 861−866, 2005.

[13] C.Y. Wen, C.H. Cheng, C.N. Jian, T.A. Nguyen, C.Y. Hsu, Y.R. Su, "A valveless micro impedance pump driven by PZT actuation," Materials Science Forum., vol. 505−507, pp.127−132, 2006.

[14] C.Y. Lee, H.T. Chang, C.Y. Wen, "A MEMS based valveless impedance pump utilizing electromagnetic actuation," J. Micromech. Microeng., vol. 18, pp 035044 (9pp), 2008.

[15] G. Liebau, "Arterielle pulsation und venöse vepulsation," Z. Gesamte Exp. Med., vol. 123, pp 71, 1954.

[16] G. Liebau, "Über ein ventilloses pumpprinzip," Naturwiss., vol.41, pp. 327, 1954.

[17] G. Liebau, "Herzpulsation und blutbewegung," Z. Gesamte Exp. Med., vol 125, pp.482, 1955.

[18] G. Liebau, "Prinzipien kombinierter ventilloser pumpen, abgeleitet vom menschlichen blutkreislauf," Naturwiss., vol. 42, pp.339, 1955.

[19] C.G. Manopoulos, D.S. Mathioulakis, S.G. Tsangaris, "One-dimensional model of valveless pumping in a closed loop and a numerical solution," Phys Fluids., Vol. 18:017106, 2006.

[20] H. Thomman, "A simple pumping mechanism in a valveless tube," Z. Angew. Math. Phys., vol.29, pp. 169–177, 1978.

[21] M. Moser, J.W. Huang, G.S. Schwarz, T. Kenner, A. Noordergraaf, "Impedance defined flow: Generalization of William Harvey's concept of the circulation – 370 years later," International Journal of Cardiovascular Medicine and Science, 1(3/4) pp.205–211, 1998.

[22] E. Jung, C. Peskin, "2-D simulations of valveless pumping using immersed boundary methods," SIAM Journal on Scientific Computing., vol. 23, pp.19–45, 2001.

[23] A. Borzi, G. Propst, "Numerical investigation of the Liebau phenomenon," Z. Angew. Math. Phys., vol. 54, pp.1050–1072, 2003.

[24] J. Ottensen, "Valveless pumping in a fluid-filled closed elastic tube system: one dimensional theory with experimental validation," Journal of Mathematical Biological, vol.46, pp.309–332, 2003.

[25] D. Auerbach, W. Moehring, M. Moser, "An analytic approach to the Liebau problem of valveless pumping," Cardiovascular Engineering, vol.4, pp.201-207, 2004.

[26] A.I. Hickerson, D. Rinderknecht, M. Gharib, "Experimental study of the behaviors of a valveless impedance pump," Experiments in Fluids, vol.38, pp.535–540, 2005.

[27] A.I. Hickerson, M. Gharib, "On the resonance of a pliant tube as a mechanism for valveless pumping," J. Fluid Mech., vol. 555, pp.141–148, 2006.

[28] I. Avrahami, M. Gharib, "Computational studies of resonance wave pumping in compliant tubes," J Fluid Mech., vol. 608, pp.139–160, 2008.

[29] C.Y. Wen, H.T. Chang, "Design and characterization of valveless impedance pumps," Journal of Mechanics, vol.25, pp.345–354, 2009.

[30] X.Y.Huang, C.Y. Wen, Z.J. Jiao, "A standing wave model for acoustic pumping effect in microchannels," Applied Acoustics, vol.71, pp.164–168, 2010.

[31] M.C. Carrozza, N. Croce, B. Magnani, P. Dario, "A piezoelectrically driven stereolithography-fabricated micropump," J. Micromech. Microeng., vol.5, pp.177–179, 1995.

[32] S. Böhm, W. Olthuis, P. Bergveld, "A plastic micropump constructed with conventional techniques and materials," Sens. Actuat. A, vol.77, pp.223–228, 1999.

[33] C. Yamahata, F. Lacharme, M.A.M Gijs, "Glass valveless micropump using electromagnetic actuation," Microelectron. Eng., vol.78–79, pp.132–7, 2005.

[34] H.T. Chang, C.Y. Lee, C.Y. Wen, BS. Hong, "Theoretical analysis and optimization of electromagnetic actuation in a valveless micro impedance pump," Microelectronics J., vol.38, pp.791–799, 2007.

[35] H.T. Chang, C.Y. Wen, C.Y. Lee, "Design, analysis and optimization of electromagnetic actuator used in micro pumps," J. Micromech. Microeng., vol.19, pp.085026, 2009.

[36] C.Y. Lee, Z.H. Chen, H.T. Chang, C.Y. Wen, C.H. Cheng, "Design and fabrication of novel micro electromagnetic actuator," Microsystem Technologies-Micro-and-Nanosystems-Information Storage and Processing Systems, vol.15, pp.1171–1175, 2009.

[37] M.C. Acero, J.A. Plaza, J. Esteve, M. Carmona, S. Marco, J. Samitier, "Design of a modular micropump based on anodic bonding," J. Micromech. Microeng., vol.7, pp.179–182, 1997.

[38] C.G. Cooney, B.C. Towe, "A thermopneumatic dispensing micropump," Sens. Actuat. A, vol.116, pp.519–524, 2004.

[39] T. Bourouina, A. Bosseboeuf, J.P. Grandchamp, "Design and simulation of an electrostatic micropump for drug-delivery applications," J. Micromech. Microeng., vol.7, pp. 186–188, 1997.

[40] M. M. Teymoori, E. Abbaspour-Sani, "Design and simulation of a novel electrostatic peristaltic micromachined pump for drug delivery applications," Sens. Actuat. A, vol.117, pp. 222–229, 2005.

[41] D. Xu, L. Wang, G.F. Ding, Y. Zhou, A.B. Yu, B.C. Cai, "Characteristics and fabrication of NiTi/Si diaphragm micropump," Sens. Actuat. A, vol.93, pp.87–92, 2001.

[42] E. Makino, T. Mitsuya, T. Shibata, "Fabrication of TiNi shape memory micropump," Sens. Actuat. A, vol.88, pp.256–262, 2001.

[43] Star Micronics Co., User's menu of SDMP305D microdiaphragm pump, pp 2–3, 2006.
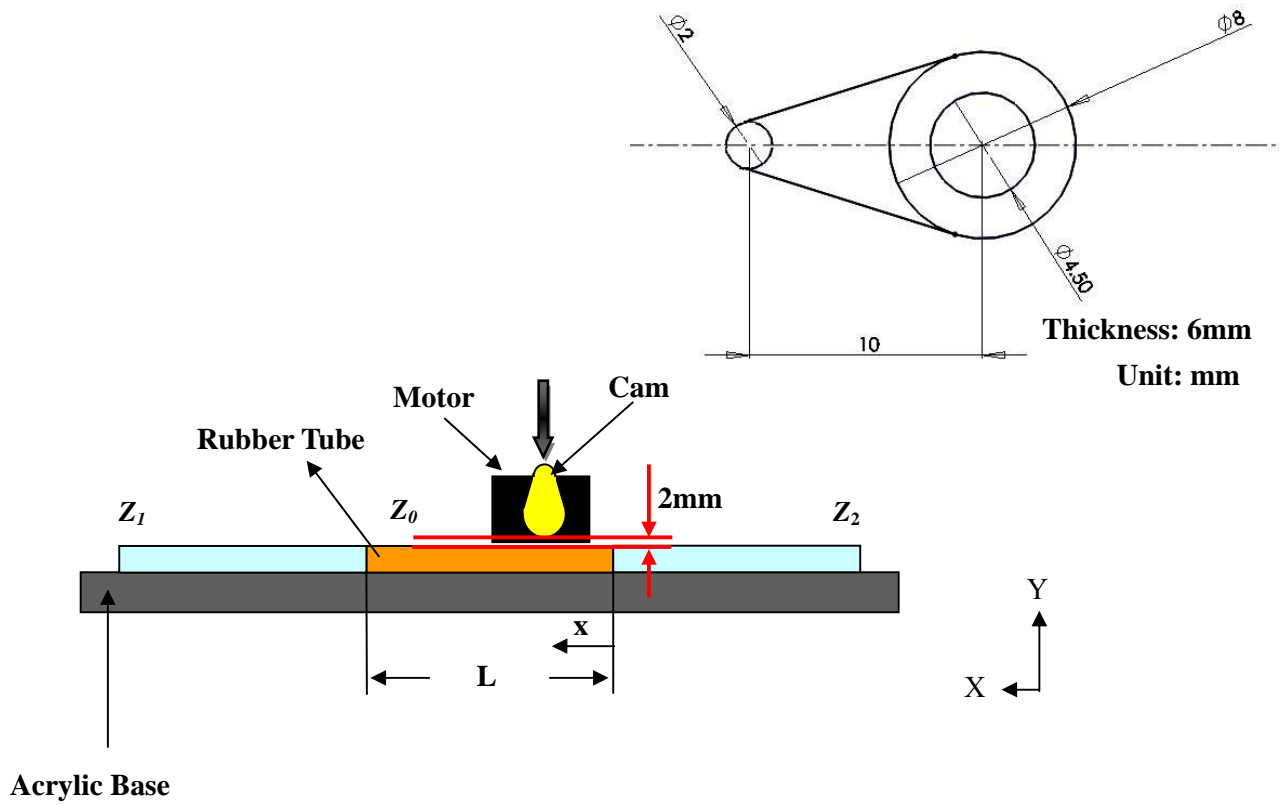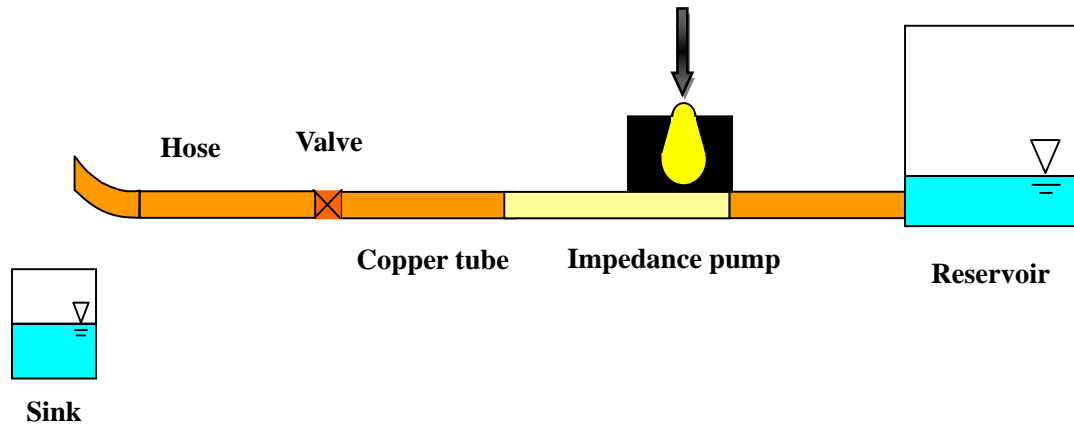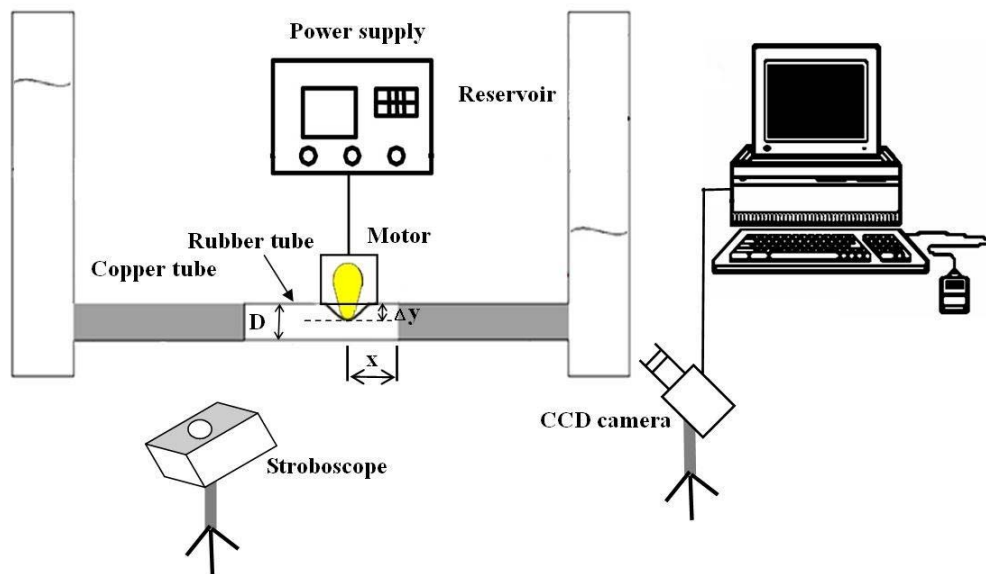
Caption of figure

Figure 1. A schematic of the impedance pump used in the current study. The big arrow above the motor–actuated cam marks the location of the excitation. The home–made PTFE cam is shown in the upper–right inset, with detailed dimensions.

Figure 2. Experimental set-up for pump performance on (a) flow rate and (b) pressure head
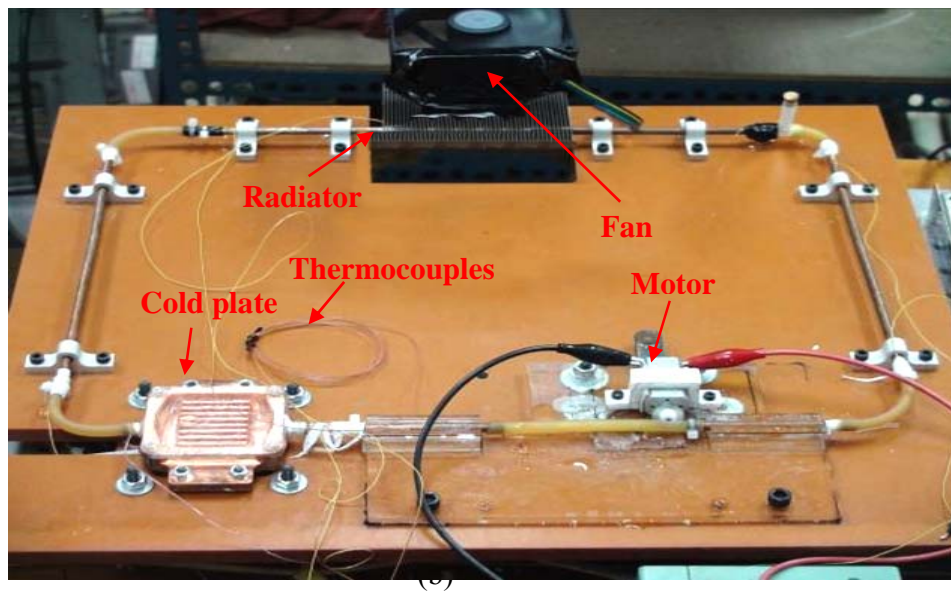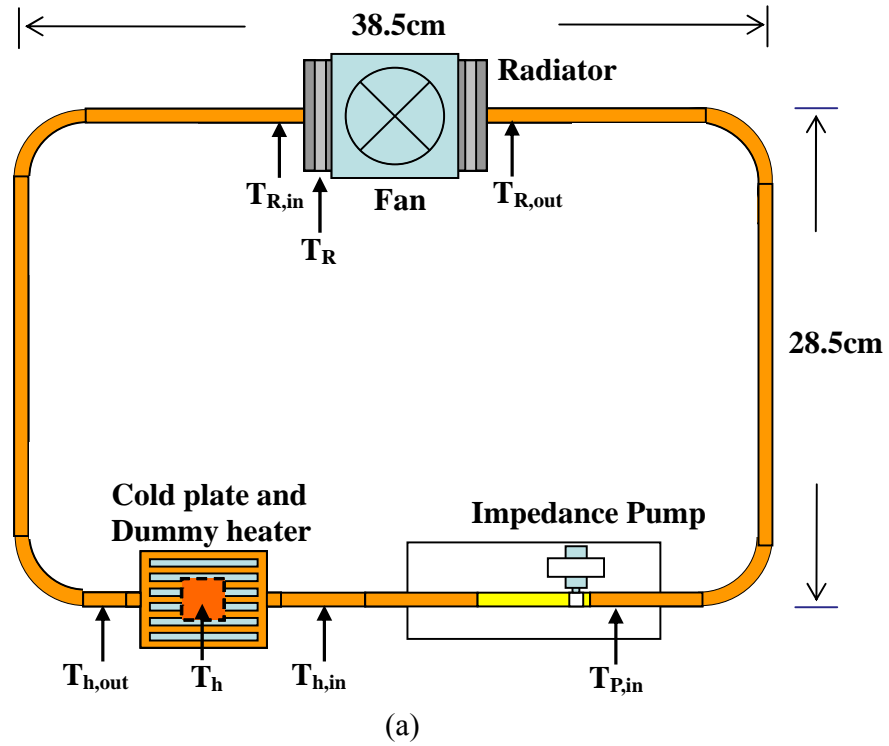
Figure 3. (a) A schematic diagram and (b) a photograph of the experimental set–up, to monitor thermal performance of the water–cooling system, in a closed loop
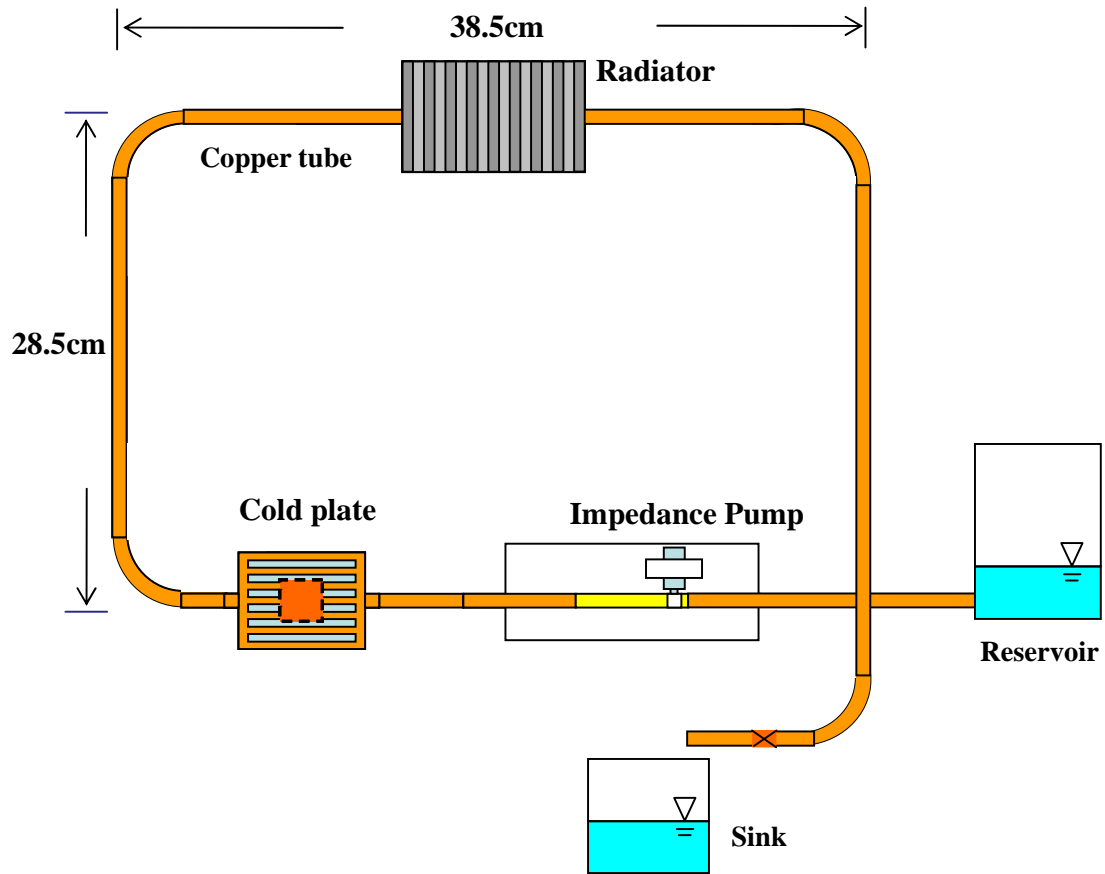
Figure 4. A schematic diagram of the experimental set–up, to monitor flow rate performance, for the water–cooling system in an open loop
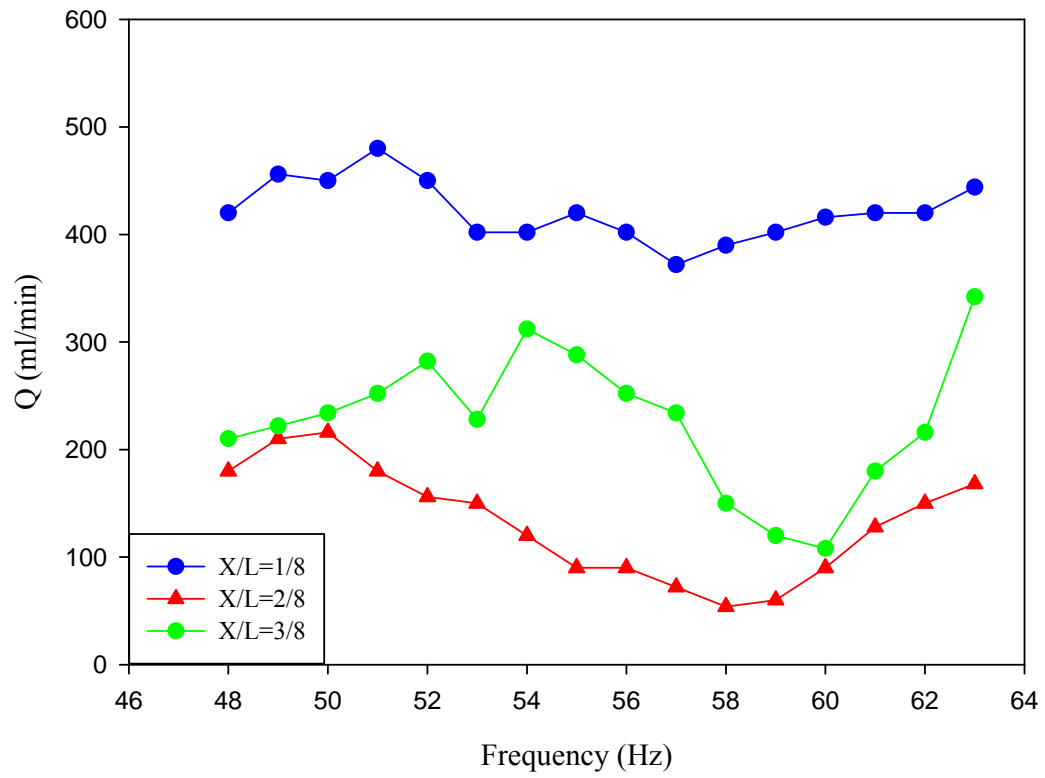
Figure 5. Measured pump flow rates at different actuation frequencies and positions

Figure 6. Variation of pressure head with elapsed time, at optimal flow rate performance, for an actuation frequency of 51 Hz and actuation position $x/L = 1/8$.

Figure 7. H–Q curve for the impedance pump, at optimal flow rate performance, at an actuation frequency of 51 Hz and actuation position $x/L = 1/8$.

Figure 8. Comparison of the measured flow rates of the water–cooling system in an open loop with that of a pump alone, at different actuation frequencies and optimal actuation position $x/L = 1/8$.

Figure 9. Thermal performance of the water–cooling system in a closed loop, at an actuation frequency of 51 Hz and actuation position $x/L = 1/8$.

Figure 1. A schematic of the impedance pump used in the current study. The big arrow above the motor–actuated cam marks the location of the excitation. The home–made PTFE cam is shown in the upper–right inset, with detailed dimensions.

(a)

(b)

Figure 2. Experimental set-up for pump performance on (a) flow rate and (b) pressure head

Figure 3. (a) A schematic diagram and (b) a photograph of the experimental set–up, to

monitor thermal performance of the water–cooling system, in a closed loop

Figure 4. A schematic diagram of the experimental set–up, to monitor flow rate performance, for the water–cooling system in an open loop

Figure 5. Measured pump flow rates at different actuation frequencies and positions

Figure 6. Variation of pressure head with elapsed time, at optimal flow rate performance,

for an actuation frequency of 51 Hz and actuation position $x/L = 1/8$.
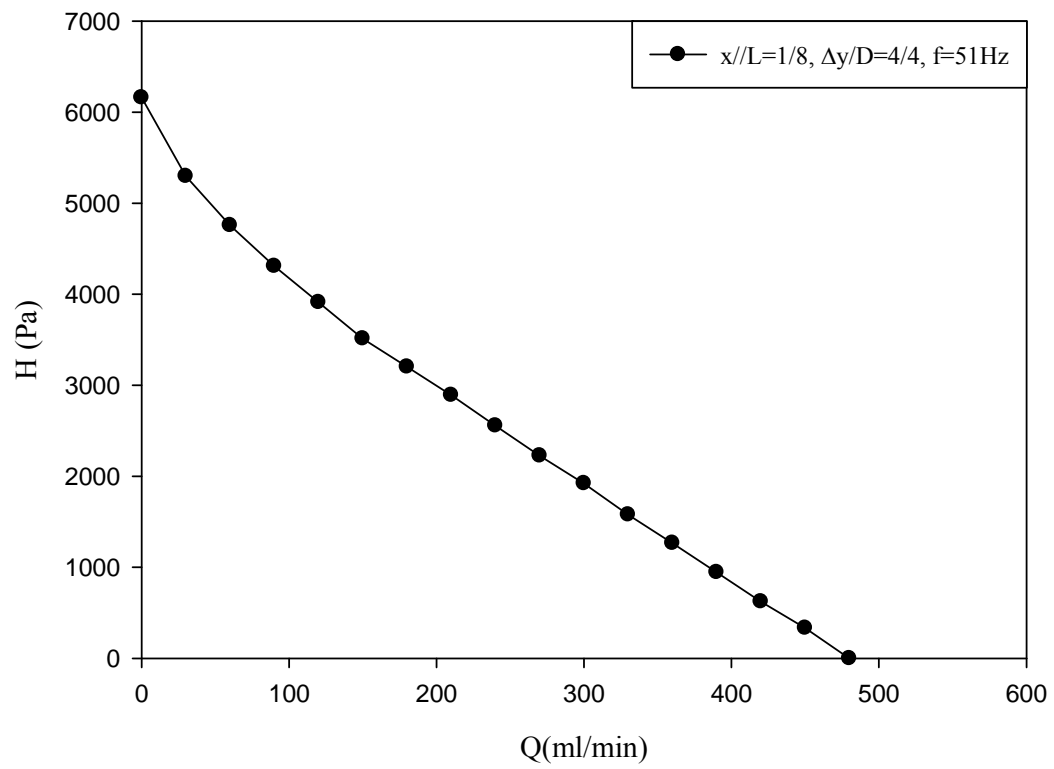
Figure 7. H–Q curve for the impedance pump, at optimal flow rate performance, at an

actuation frequency of 51 Hz and actuation position $x/L = 1/8$.
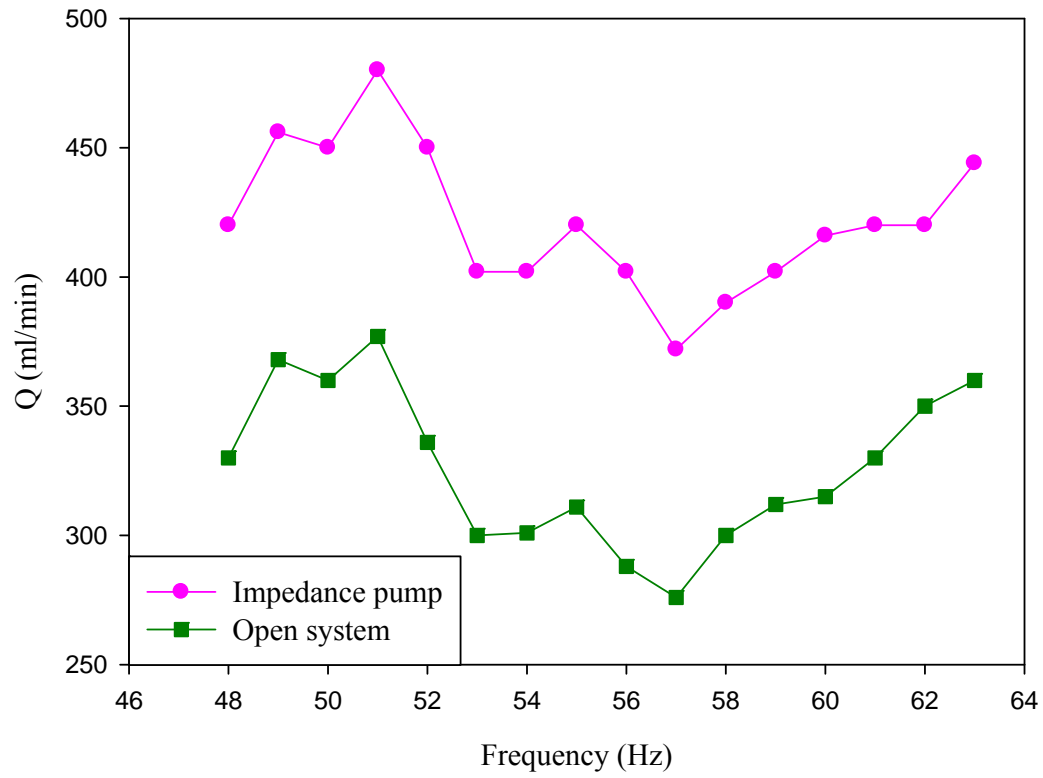
Figure 8. Comparison of the measured flow rates of the water–cooling system in an open

loop with that of a pump alone, at different actuation frequencies and optimal
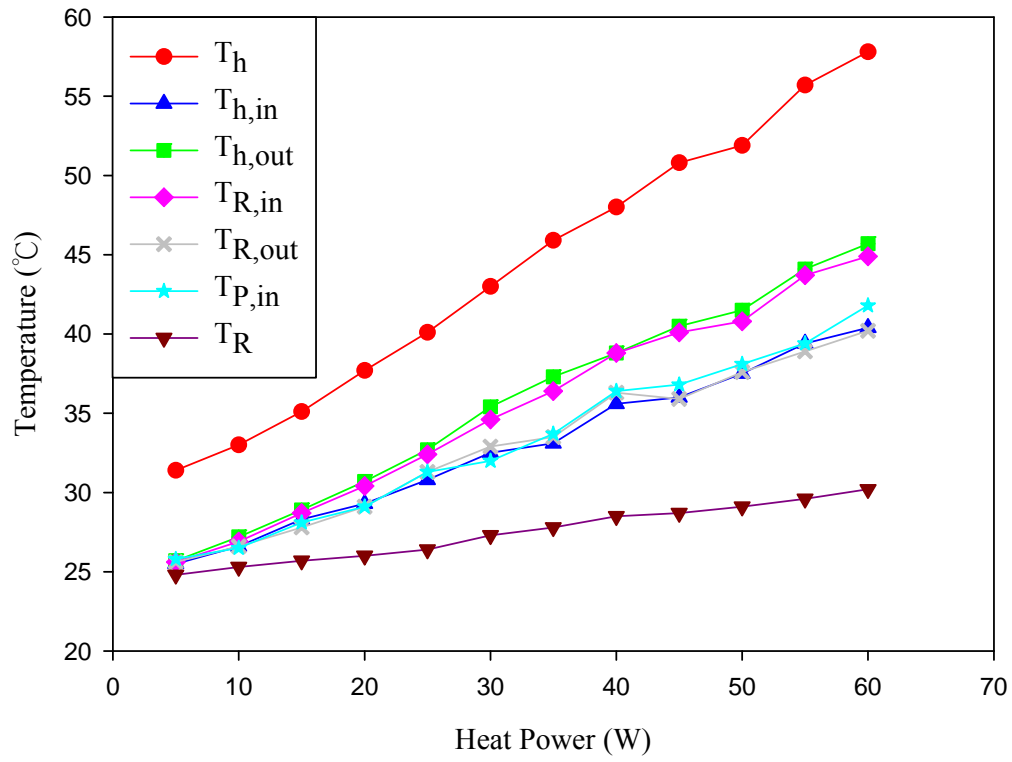
actuation position $x/L = 1/8$.

Figure 9. Thermal performance of the water–cooling system in a closed loop, at an actuation frequency of 51 Hz, actuation position $x/L = 1/8$ and pumping flow rate of 375 ml/min.